# Interdot carrier and spin dynamics in a two-dimensional high-density quantum-dot array of InGaAs with quantum dots embedded as local potential minima

**Satoshi Hiura[1], Masayuki Urabe[1], Kazuki Takeishi[1], Kodai Itabashi[1], Junichi Takayama[1], Takayuki Kiba[2], Kazuhisa Sueoka[1] and Akihiro Murayama[1]**

[1] Graduate School of Information Science and Technology, Hokkaido University, Kita 14, Nishi 9, Kita-ku, Sapporo, Japan
[2] Kitami Institute of Technology, 165 Koen-cho, Kitami, Japan

E-mail: hiura@ist.hokudai.ac.jp

**Abstract.** Interdot carrier and spin dynamics were studied in a two-dimensional array of high-density small quantum dots (SQDs) of InGaAs with an average diameter of 16 nm and a sheet density of 1.2 $\times 10^{11}$cm$^{-2}$, in which 24 nm diametric large QDs (LQDs) were embedded as local potential minima. We observed a delayed photoluminescence (PL) rise from the lower-lying LQD states and a considerably faster PL decay from the higher-lying SQD states, indicating carrier transfer from the two-dimensionally coupled SQDs into the LQDs. In addition, inverse carrier tunneling from the LQDs into the SQDs was thermally induced, which is characterized by the thermal activation energy between the LQDs and SQDs. Moreover, circularly polarized transient PL behavior from the SQD states exhibits a suppression of the spin polarization decay in the initial time region, depending on the excited spin density. This tentatively suppressed spin relaxation can be quantitatively explained by selective interdot transfer of minority-spin electrons from the SQDs into LQDs, when the majority spin states in both QDs are sufficiently populated by excited spins. These findings indicate that the high-density SQDs behave as the main emitters with suppressed spin relaxation, while the scattered LQDs with lower potential behave as the receivers of minority-spin electrons.

Submitted to: *Semicond. Sci. Technol.*

## 1. Introduction

Self-assembled semiconductor quantum dots (QDs) have been extensively studied for the future development of ultralow-power-consumption opto-electric and opto-spintronic devices, as they can strongly confine carriers [1]. In particular, spins in semiconductor QDs are the main subject of ongoing research owing to their weak interaction with their solid-state environment, resulting in long spin lifetimes [2, 3, 4, 5] and their potential application in spintronics and quantum information technology [6]. There is also a great interest in the carrier and spin dynamics present in QDs, because these understandings could provide new proposed QD geometries for designing high-performance QD-based devices. In general, the increase of the QD density is required for achieving a higher luminance and optical gain [7] while developing QD-based spin-functional optical devices, such as spin-polarized light-emitting diodes [8, 9, 10] or laser diodes [11]. For the spin-related properties, high-density QDs have a significant potential of higher spin-polarized emission owing to their faster capture of electron spins from a three-dimensional semiconductor barrier while maintaining high spin polarization [12]. However, there remains a lack of understanding of the carrier and spin dynamics in high-density QD ensembles due to the emissions from these ensemble states including various contributions, such as differently-sized QD states and the influence of interdot coupling between the carrier wavefunctions of neighboring QDs. If two-dimensional high-density QDs are separated into two types according to their size, one can obtain a new understanding of the effect of each spin functionality on the total QD emission, which can pave the way for the development of new nanosystems with novel spin functionalities, such as a strong suppression of spin relaxation in QD ensembles.

The lateral dot size and sheet dot density of semiconductor QDs depend on the growth conditions, such as arsenic pressure [13]. The lateral dot size becomes smaller and the sheet dot density increases with the increase of the arsenic pressure during QD growth, owing to the suppression of surface migration of the species. In addition, the increased arsenic pressure induces coalescent QD growth, i.e., the growth of large-sized QDs. These facts indicate that controlling the arsenic pressure during QD growth has a significant potential for intentionally controlling the lateral QD geometries, such as their size, sheet density, size distribution, and dot-dot distance. In this work, we have grown two-dimensional arrays of high-density small InGaAs QDs surrounding large QDs by controlling the arsenic pressures based on a previous report [13]. This newly grown multiple QD nanosystem exhibits tentative suppression of spin polarization decay in the small QD emissive states, caused by the selective interdot transfer of minority-spin electrons into the large QD states. This novel QD nanosystem has a great potential for the future development of high-density QDs, maintaining high spin polarization during light emission.

## 2. Experimental procedure

Optically active layers of $In_{0.5}Ga_{0.5}As$ QDs with 6 ML were grown on GaAs(100) substrates with GaAs buffer layers by molecular beam epitaxy under growth conditions similar to those used previously [14, 15]. Two types of $In_{0.5}Ga_{0.5}As$ QDs were grown at a growth rate of 0.20 ML/s under arsenic pressures of 2 $\times 10^{-6}$ and 3 $\times 10^{-6}$ Torr, and subsequently capped with 40 nm-thick GaAs layer. Additional QDs were grown on the capping layer to observe the QD structures by atomic force microscopy (AFM). Photoluminescence (PL) spectroscopy including circularly polarized properties and time-resolved PL (TRPL) measurements were performed, aided by a rate-equation fit analysis using a method described previously [14, 15]. Furthermore, to investigate the potential profile and eigenvalues of the electron and hole wavefunctions of the $In_{0.5}Ga_{0.5}As$ QDs of various sizes, three-dimensional calculations of their band structures and the wavefunctions of the carriers inside them were carried out using the nextnano$^3$ software package [16], taking into account the shape of the dots, their composition, and strain. Here, the transient behavior of QD-PL was focused predominantly. From the rise times and the decay times of the QD-PL, we discuss the interdot carrier dynamics, as well as the carrier injection or relaxation dynamics. We also explore the temperature dependence of the interdot carrier transfer. Moreover, we investigate the transient behavior of the circular polarization of QD-PL, which reflects the time-dependent electron-spin polarization of the QD emissive states. Interdot spin dynamics based on the decay properties of the time-dependent

circular polarization are discussed using a rate-equation fit analysis that takes the effective interdot spin transfer time into account.

## 3. Results and discussion

### *3.1. AFM analysis of the QD nanostructures*

Figures 1(a) and 1(b) show AFM images of the QDs grown at a growth rate of 0.20 ML/s under arsenic pressures of 2 $\times 10^{-6}$ and 3 $\times 10^{-6}$ Torr, respectively. The sheet densities of the QDs were estimated as approximately 8.0 $\times 10^{10}$ and 1.2 $\times 10^{11}$cm$^{-2}$. Hereinafter, these QDs are denoted as high-density QDs (HQDs) and ultra-high density QDs (UHQDs). The higher sheet density of the UHQD sample can be derived from the suppression of the surface migration of In and Ga species under the higher arsenic pressure [13, 17]. Figure 1(c) shows the distribution of the lateral dot diameter of the HQDs and UHQDs, obtained from the AFM analysis of the QD nanostructures. The HQDs exhibit a conventional Gaussian-like size distribution, similar to a previously observed one [15], while the size distribution of UHQDs indicates the coexistence of small QDs (SQDs) and large QDs (LQDs) with a number ratio of 7:1. The higher arsenic pressure during QD growth can induce both the decrease of the QD size and the coalescence of SQDs, i.e., the growth of LQDs [13]. Figure 1(d) shows an enlarged three-dimensional AFM image (150 $\times$ 150 nm$^2$) of the UHQDs, where an LQD is closely surrounded by a two-dimensional array of SQDs with center-to-center distances below 30 nm. This means that the shortest base-to-base distance between an SQD and an LQD is below 10 nm considering the average SQD and LQD sizes of 16 and 24 nm obtained through AFM analysis. The SQDs are close to each other, characterized by shorter distances. In such a high-density QD system, the electron wavefunctions among neighboring QDs are coupled, which can largely affect the carrier dynamics and optical properties of QDs [18, 19, 20, 21]. In the following, the UHQD sample is mainly discussed, because this QD ensemble shows the unique interdot carrier and spin dynamics, as compared to the well-known dynamics in the HQD sample.

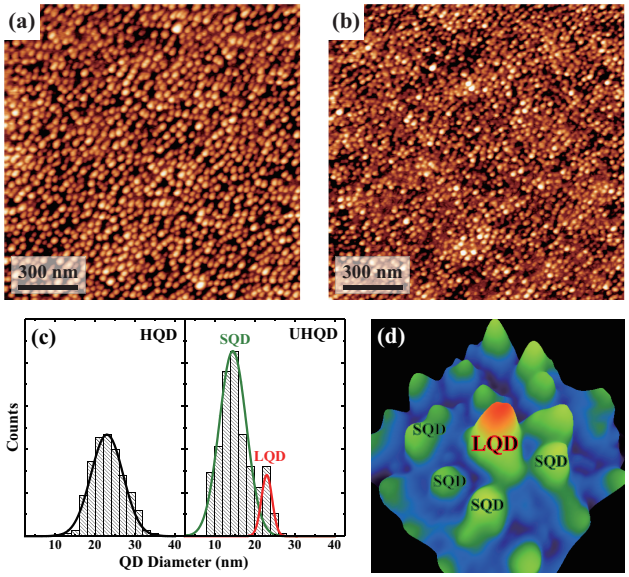


**Figure 1.** (a), (b) AFM images of $In_{0.5}Ga_{0.5}As$ QDs grown at a growth rate of 0.20 ML/s under arsenic pressures of 2 $\times 10^{-6}$ and 3 $\times 10^{-6}$ Torr, respectively. (c) Distribution of the lateral dot diameter of the HQDs (left) and UHQDs (right) shown in (a) and (b). (d) Enlarged three-dimensional AFM image (150 $\times$ 150 nm$^2$) of UHQDs, indicating a laterally coupled QD system, where an LQD is closely surrounded by a two-dimensional array of SQDs.

### *3.2. Interdot carrier transfer dynamics*

PL spectrum of UHQD sample measured at 6 K under an excitation power of 13 mW as a function of photon energy is shown in Fig. 2(a). This spectrum can be decomposed into two components, as shown by the red and green lines. The PL emission from the lower state (LS) is relatively smaller than the one from the higher state (HS). We performed three-dimensional calculations of the electron and hole wavefunctions for $In_{0.5}Ga_{0.5}As$ QDs to reveal the LS and HS. Figure 2(b) shows the calculation results of the potential profile and the ground states of the electron and hole wavefunctions for $In_{0.5}Ga_{0.5}As$ QDs with two different base lengths. Here, these values were set to 24 and 16 nm, according to the lateral diameters of the LQDs and SQDs obtained through AFM analysis. It was found that LQDs and SQDs can lead to ground state PL energies of $\sim$1.28 and $\sim$1.32 eV. These energy values agree well with the LS and HS of UHQDs, which indicates that the PL emissions observed at the LS and HS originate from the ground states of the LQDs and SQDs, respectively. Here, we discuss the screening of PL peak of LQD around 1.28 eV. The overwhelming majority of SQD in UHQDs described above results in the pronounced PL component centered around 1.32 eV, while the much lower number of LQD has a significantly weaker contribution to the total PL emission. Moreover, QD-PL spectra actually consist of a superposition of transitions between various electron and hole states of differently-sized QDs, and thus a decomposed PL peak of LQD around 1.28 eV can be hidden in the overall PL spectrum.

We performed TRPL measurements of the UHQDs to further clarify the LS and HS described above. Figure 2(c) shows the normalized TRPL curves measured at 6 K under an excitation power of 10

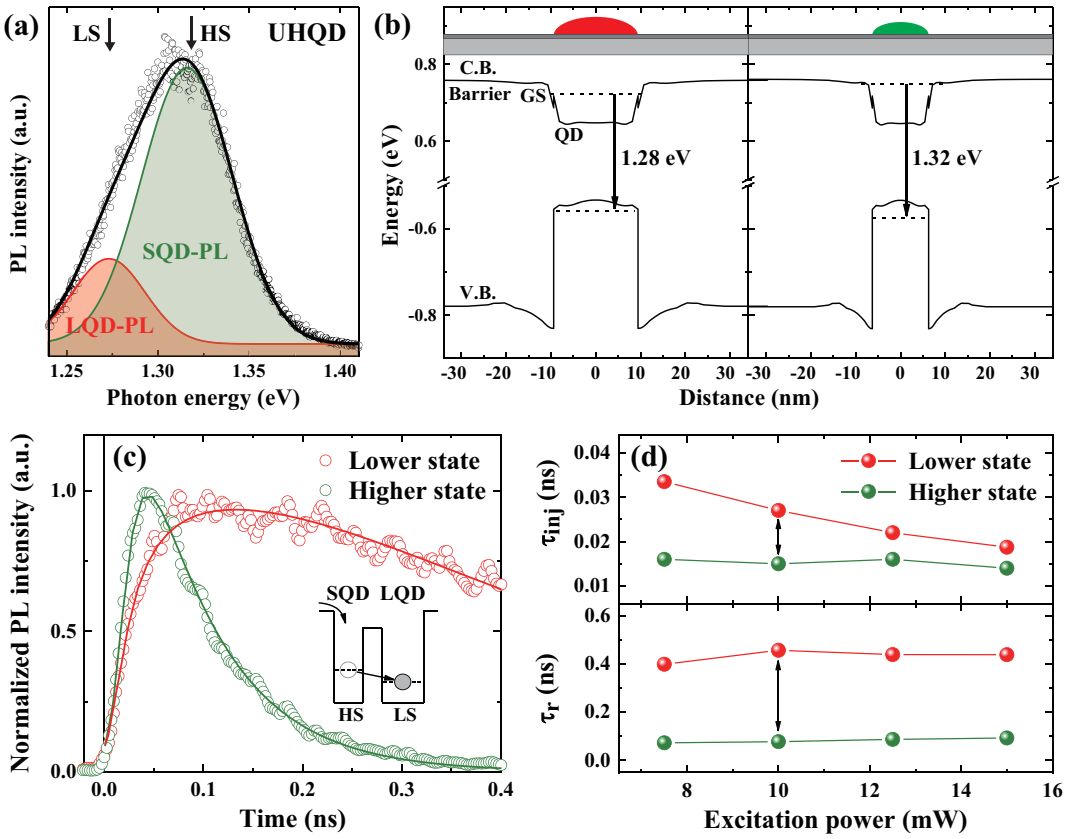


**Figure 2.** (a) PL spectrum of UHQDs measured at 6 K under an excitation power of 13 mW. This spectrum can be decomposed into two components. (b) Three-dimensional calculation results of the potential profile and ground state (GS) of the electron and hole wavefunctions for $In_{0.5}Ga_{0.5}As$ QDs with base lengths of 24 nm (left) and 16 nm (right), whose values are used according to the lateral dot diameters of LQD and SQD shown in Fig. 1(c). (c) Normalized TRPL curves measured at 6 K under an excitation power of 10 mW for the lower state (LS) and higher state (HS) indicated in Fig. 2(a), best fitted by the rate-equations (solid lines). The inset shows a simple model of interdot carrier tunneling from the SQDs into LQDs. (d) Excitation power dependence of the time constants for carrier injection from the barrier into the QD levels, $\tau_{inj}$, and energy relaxation from the QD levels, $\tau_r$, deduced from the rate-equation fit of the LS and HS.

mW of the LS and HS. The TRPL curve of the LS indicates a different behavior of the PL rise compared to the one of HS. We can see the delayed rise in the TRPL curve of the LS. This delayed PL rise is commonly observed in bilayer asymmetric InAs/GaAs QDs [20] and vertically stacked asymmetric pairs of InP QDs [21] with a thin spacer layer, where interdot carrier tunneling can occur. This TRPL behavior can be understood via the delayed carrier filling of the large dots by the small dots owing to interdot carrier tunneling. Since our UHQD sample is composed of SQDs and LQDs close to each other, as described above, interdot carrier tunneling from the SQDs into the LQDs can be applied to the UHQDs, as shown in the inset of Fig. 2(c). We also carried out rate-equation fit analysis of the TRPL curves under various excitation powers to understand the dependence of interdot carrier transfer on the excited carrier density. Figure 2(d) shows the excitation power dependence of the time constants of carrier injection from the barrier into the QD levels, $\tau_{inj}$, and energy relaxation from the QD levels, $\tau_r$, deduced from the rate-equation fit of the LS and HS. The significant difference in the $\tau_{inj}$ for the lower excitation power originates from the slower injection process into the LQDs via the SQDs [22]. However, the difference decreases with the increase of the excitation power. The faster $\tau_{inj}$ under higher excitation powers for the LS can be due to the increased number of carriers directly injected from the barrier or the wetting layer without interdot tunneling process. In contrast, the difference in the $\tau_r$ remains significant, being almost independent of excitation power. The much faster $\tau_r$ of the HS originates from the presence of extra decay channels for the SQDs, i.e., interdot carrier tunneling into the LQDs in addition to neighboring SQDs.

We also investigated the temperature dependence of interdot carrier transfer in UHQDs. Figure 3(a) shows the PL spectra of HQDs and UHQDs measured at various temperatures. Here, the HQD sample was

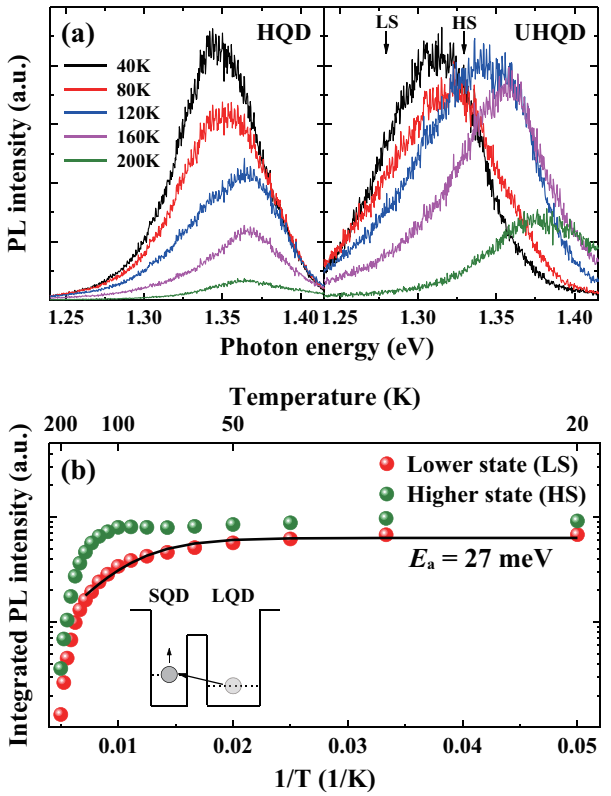


**Figure 3.** (a) PL spectra of HQDs (left) and UHQDs (right) measured at various temperatures. The lower state (LS) and higher state (HS) of the UHQDs are indicated by black arrows. (b) Temperature dependence of the integrated PL intensity of the LS and HS together with the Arrhenius plot of the LS obtained at a temperature range of 20–140 K. The inset shows a simple model of the thermally activated carrier tunneling from the LQDs into SQDs and the thermal excitation of SQDs into the higher energy states.

used as conventional QDs for reference. The result of the HQDs shows a well-known monotonic decrease of the PL intensity with the temperature increase, which is independent of energy. This behavior can be understood through carrier escape out of the QDs, i.e., thermal activation into the barrier or nonradiative centers [23]. In contrast, the UHQDs show a clear evidence of the energy-dependent PL behavior in the temperature range of 40–120 K. Figure 3(b) shows the temperature dependence of the integrated PL intensity for the LS and HS. The result for the LS indicates a gradual decrease of PL intensity, while the one for the HS shows a relatively-constant PL intensity at a temperature of 20–120 K. This energy dependence of the temperature-dependent PL intensity can be understood by the thermally activated carrier tunneling from the LQDs into the SQDs, although a part of the carriers in the SQDs is also thermally activated into the higher energy states, as shown in the inset of Fig. 3(b). The thermal activation energy $E_a$ of the LS is estimated as 27 meV, whose value well corresponds to the energy difference of 26 meV between the ground states of $In_{0.5}Ga_{0.5}As$ QDs with base lengths of 24 and 16 nm. Note that the PL data measured above 140 K are not used when calculating the thermal activation energy, as the PL intensity rapidly decreases above 140 K owing to not only the thermal activation into SQD states but also the thermal activation into the higher energy states inside the LQDs. These excitation power dependences of the energy-dependent TRPL shown in Fig. 2 and the temperature dependence of the energy-dependent PL shown in Fig. 3 clearly revealed that the LS and HS correspond to the LQD states and to two-dimensionally coupled SQD (2D SQD) states, respectively.

### *3.3. Interdot spin transfer dynamics*

We next focus on the interdot spin transfer dynamics in UHQDs. Figure 4(a) shows the circularly polarized PL spectra of UHQDs measured at 6 K under an excitation power of 12.5 mW and the corresponding circular polarization degree (CPD) as a function of photon energy. Here, the CPD is defined as $(I_{\sigma+} - I_{\sigma-})/(I_{\sigma+} + I_{\sigma-})$, where $I_{\sigma+}$ and $I_{\sigma-}$ denote the intensities of the $\sigma^+$- and $\sigma^-$-polarized PL signals, respectively. We can see stronger PL and much higher CPD values for the 2D SQD states compared to the LQD states. Figure 4(b) shows the circularly polarized TRPL curves and the corresponding CPD for the LQD and 2D SQD states. The time-dependent CPD for the LQD states shows a rapid decay indicating a spin-state filling at QD states [24, 14], which is well expressed by a rate-equation fit based on previous reports (see the solid lines) [14, 15]. It should be noted that the time-dependent CPD for 2D SQD states shows a tentatively slow decaying feature in the initial time region and two components at the CPD decay times of 0.96 and 0.34 ns are observed. Taking into account that the spin relaxation time is equal to twice the CPD decay time [5], the first and second components of the spin relaxation time correspond to 1.9 and 0.7 ns, respectively. The faster value of 0.7 ns is in good agreement with the previous ones in InGaAs/GaAs QDs [14, 15], while the much slower value of 1.9 ns cannot be explained in conventional InGaAs QD systems. We recently observed a similar behavior with tentatively persistent CPD features in laterally coupled InGaAs QDs with the QDs well-ordered along one direction like a one-dimensional chain [25]. The non-monotonic CPD feature is explained by selective interdot transfer of minority-spin electrons among the QDs [26]. Therefore, this tentative suppression of CPD decay observed for UHQDs can be understood by a similar mechanism of interdot spin transfer, i.e., selective interdot transfer of minority-spin electrons

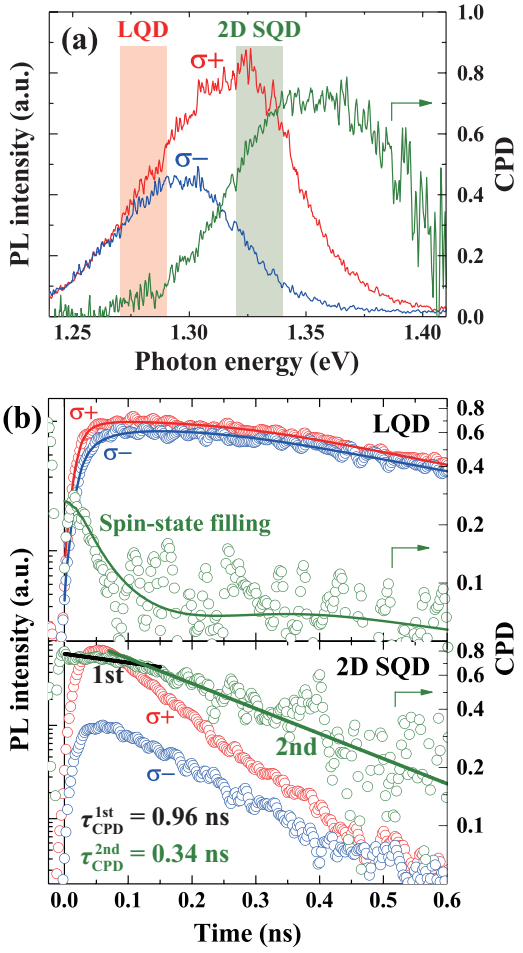


**Figure 4.** (a) Circularly polarized PL spectra and the corresponding CPD measured at 6 K under an excitation power of 12.5 mW for UHQDs. The red and green rectangles show the energy windows for LQD and 2D SQD states, respectively. (b) Circularly polarized TRPL curves and the corresponding CPD for LQD (above) and 2D SQD (below) states indicated by the red and green rectangles in (a). The solid lines for the LQD indicate the best fitting calculation result of the rate-equations. The solid lines for the 2D SQD indicate the fit results for the single exponential decay of the first and second components of the CPD decay.

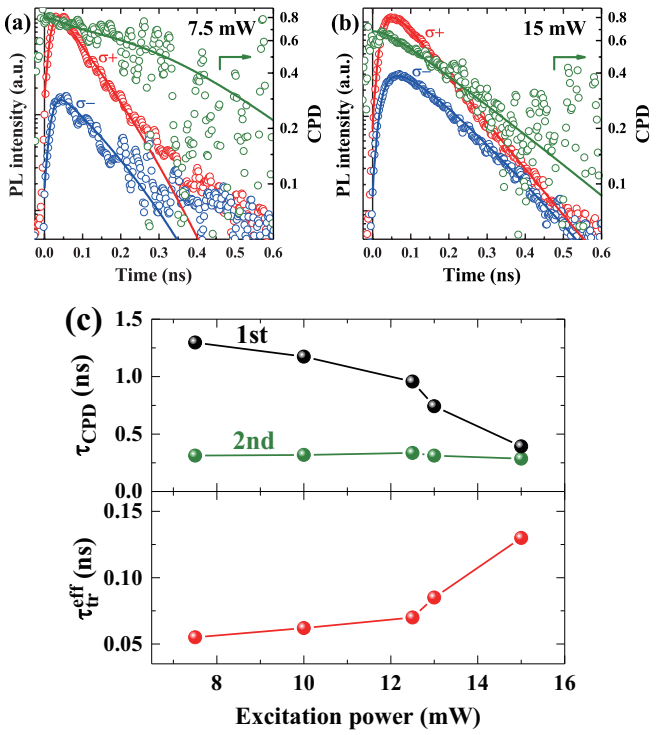


**Figure 5.** Circularly polarized TRPL curves and the corresponding CPD, best fitted by the rate-equations (solid lines), taking into account an effective interdot spin transfer time for 2D SQD states measured under excitation powers of (a) 7.5 and (b) 15 mW. (c) Excitation power dependence of the first and second components of the CPD decay time $\tau_{\mathrm{CPD}}$ and effective interdot spin transfer time $\tau_{\mathrm{tr}}^{eff}$ deduced from the rate-equation fit of the 2D SQD states.

from the SQDs into LQDs.

We also performed circularly polarized TRPL measurements under various excitation powers to understand the dependence of interdot spin transfer on the excited spin density. To quantitatively analyze the TRPL curves, rate-equation fit analysis that takes into account the effective rate of interdot spin transfer was employed based on the recent report [25]. This rate-equation model assumes two types of QD levels, the higher-energy level in the SQDs and the lower-energy level in the neighboring LQDs. In addition, an effective interdot transfer time $\tau_{\mathrm{tr}}^{eff}$, which reflects an effective transfer time from the SQDs into the LQDs, is introduced. Here, the spin injection process into the LQD level via the SQD level is assumed, owing to the lower capture rate of carriers from the barrier to the LQDs [22]. The remaining assumptions and the applied parameters are based on previous reports [14, 15]. Figures 5(a) and 5(b) show the circularly polarized TRPL curves and the corresponding CPDs for the 2D SQD states measured under excitation powers of 7.5 and 15 mW, respectively. The suppression of CPD decay is clearly observed in the initial time region under the lower excitation power of 7.5 mW, while the feature almost disappears and a single-exponential-like decay of the CPD is observed under the higher excitation power of 15 mW. This excitation-density-dependent behavior of the transient CPD demonstrates the dependence of interdot spin transfer on the excited spin density. Figures 5(a) and 5(b) also show the rate-equation fit results for these circularly polarized TRPL, with a convolution calculation of the instrumental time-response curve of the excitation laser pulse. The tentative suppression of CPD decay, as well as the circularly polarized transient PL intensities can be well expressed by tuning the interdot transfer parameter $\tau_{\mathrm{tr}}^{eff}$.

Figure 5(c) shows the excitation power dependence of the first (slower) and second (faster) components of the CPD decay time $\tau_{\rm CPD}$ and the effective interdot spin transfer time $\tau_{\rm tr}^{eff}$, deduced from the rate-equation fit of the 2D SQD states. For the lower excitation power of 7.5 mW, we can see a large difference between the slower and faster CPD decay times of 1.30 and 0.31 ns. In this case, the fastest $\tau_{\rm tr}^{eff}$ of 55 ps is also obtained, which means that interdot spin transfer becomes dominant. The selective interdot transfer of minority-spin electrons from the SQDs into the LQDs is actively induced by the moderate strength of the spin-state filling of the LQD states, resulting in the tentative suppression of the CPD decay. However, the difference in the $\tau_{\rm CPD}$ becomes smaller with the increase of the excitation power, followed by the gradual increase of the $\tau_{\rm tr}^{eff}$ values. This variation means that the spin-state filling effect of the LQD states becomes significant owing to the limited number of LQDs, which can prevent the interdot transfer of minority-spin electrons from the SQDs. However, we can still see a subtle difference in the $\tau_{\rm CPD}$ even under the highest excitation power of 15 mW. Interdot spin transfer among neighboring SQDs with slightly different sizes might also contribute to the small suppression of the CPD decay, even after the strong spin-state filling of the LQD states. As a whole, these results indicate that high-density SQDs behave as the main emitters with suppressed spin relaxation, while the low-density LQDs with lower potentials behave as the receivers of minority-spin electrons.

## 4. Conclusions

Interdot carrier and spin dynamics in a two-dimensional array of high-density InGaAs SQDs surrounding the LQDs embedded as local potential minima were systematically studied. A delayed PL rise for the lower-lying LQD state and a significantly faster PL decay for the higher-lying SQD state indicate a carrier transfer from the two-dimensionally coupled SQDs into the LQDs. In addition, inverse carrier tunneling from the LQDs into the SQDs was found to be thermally induced, which is clearly characterized by the thermal activation energy between the SQDs and LQDs. The circularly polarized transient PL from the SQD states shows a tentative suppression of spin polarization decay in the initial time region, depending on the excited spin density. This behavior can be quantitatively understood by the selective interdot transfer of minority-spin electrons from the SQDs into the LQDs. These results revealed that the high-density SQDs behave as the main emitters with suppressed spin relaxation, while the low-density LQDs behave as the receivers of minority-spin electrons. These findings provide insights for developing novel spin functionalities into higher spin-polarized emission of laterally coupled InGaAs QDs by properly controlling the ratio of the sheet density of the LQDs and SQDs, and the energy difference between these differently-sized QD states.

## Acknowledgments

This study was supported by the Japan Society for the Promotion of Science, Grant-in-Aid for Scientific Research (S) (KAKENHI No. 16H06359), Grant-in-Aid for Research Activity start-up (KAKENHI No. 17H06482), and bilateral program.

## References

[1] Arakawa Y and Sakaki H 1982 Multidimensional quantum well laser and temperature dependence of its threshold current *Appl. Phys. Lett.* **40** 93941

[2] Khaetskii A V and Nazarov Y V 2000 Spin relaxation in semiconductor quantum dots *Phys. Rev. B* **61** 1263942

[3] Paillard M, Marie X, Renucci P, Amand T, Jbeli A and Grard J M 2001 Spin Relaxation Quenching in Semiconductor Quantum Dots *Phys. Rev. Lett.* **86** 16347

[4] Borri P, Langbein W, Schneider S, Woggon U, Sellin R, Ouyang D and Bimberg D 2001 Ultralong Dephasing Time in InGaAs Quantum Dots *Phys. Rev. Lett.* **87** 157401

[5] Tackeuchi A, Ohtsubo R, Yamaguchi K, Murayama M, Kitamura T, Kuroda T and Takagahara T 2004 Spin relaxation dynamics in highly uniform InAs quantum dots *Appl. Phys. Lett.* **84** 35768

[6] Loss D and DiVincenzo D P 1998 Quantum computation with quantum dots *Phys. Rev. A* **57** 120

[7] Amano T, Sugaya T and Komori K 2006 Characteristics of 1.3 $\mu$ m quantum-dot lasers with high-density and high-uniformity quantum dots *Appl. Phys. Lett.* **89** 171122

[8] Chye Y, White M E, Johnston-Halperin E, Gerardot B D, Awschalom D D and Petroff P M 2002 Spin injection from (Ga,Mn)As into InAs quantum dots *Phys. Rev. B* **66** 201301

[9] Li C H, Kioseoglou G, van't Erve O M J, Ware M E, Gammon D, Stroud R M, Jonker B T, Mallory R, Yasar M and Petrou A 2005 Electrical spin pumping of quantum dots at room temperature *Appl. Phys. Lett.* **86** 132503

[10] Lombez L, Renucci P, Braun P F, Carrère H, Marie X, Amand T, Urbaszek B, Gauffier J L, Gallo P, Camps T, Arnoult A, Fontaine C, Deranlot C, Mattana R, Jaffrès H, George J-M and Binh P H 2007 Electrical spin injection into p-doped quantum dots through a tunnel barrier *Appl. Phys. Lett.* **90** 81111

[11] Basu D, Saha D, Wu C C, Holub M, Mi Z and Bhattacharya P 2008 Electrically injected InAs/GaAs quantum dot spin laser operating at 200K *Appl. Phys. Lett.* **92** 91119

[12] Chauhan K N, Riffe D M, Everett E A, Kim D J, Yang H and Shen F K 2013 Carrier capture dynamics of single InGaAs/GaAs quantum-dot layers *J. Appl. Phys.* **113** 203710

[13] Yamaguchi K, Yujobo K and Kaizu T 2000 Stranski-Krastanov Growth of InAs Quantum Dots with Narrow Size Distribution *Jpn. J. Appl. Phys.* **39** L12458

[14] Kiba T, Yang X, Yamamura T, Kuno Y, Subagyo A, Sueoka K and Murayama A 2013 Temperature dependence of the dynamics of optical spin injection in self-assembled InGaAs quantum dots *Appl. Phys. Lett.* **103** 82405

[15] Yamamura T, Kiba T, Yang X, Takayama J, Subagyo A, Sueoka K and Murayama A 2014 Growth-temperature dependence of optical spin-injection dynamics in self-assembled InGaAs quantum dots *J. Appl. Phys.* **116** 94309

[16] Birner S, Zibold T, Andlauer T, Kubis T, Sabathil M, Trellakis A and Vogl P 2007 nextnano: General Purpose 3-D Simulations *IEEE Trans. Electron Devices* **54** 213742

[17] Yamaguchi K and Kanto T 2005 Self-assembled InAs quantum dots on GaSb/GaAs(001) layers by molecular beam epitaxy *J. Cryst. Growth* **275** e226973

[18] Tackeuchi A, Nakata Y, Muto S, Sugiyama Y, Usuki T, Nishikawa Y, Yokoyama N and Osamu Wada O W 1995 Time-Resolved Study of Carrier Transfer among InAs/GaAs Multi-Coupled Quantum Dots *Jpn. J. Appl. Phys.* **34** L1439

[19] Mazur Y I, Tomm J W, Petrov V, Tarasov G G, Kissel H, Walther C, Zhuchenko Z Y and Masselink W T 2001 Staircase-like spectral dependence of ground-state luminescence time constants in high-density InAs/GaAs quantum dots *Appl. Phys. Lett.* **78** 32146

[20] Mazur Y I, Wang Z M, Tarasov G G, Salamo G J, Tomm J W, Talalaev V and Kissel H 2005 Nonresonant tunneling carrier transfer in bilayer asymmetric InAs/GaAs quantum dots *Phys. Rev. B* **71** 235313

[21] Reischle M, Beirne G J, Robach R, Jetter M, Schweizer H and Michler P 2007 Nonresonant tunneling in single asymmetric pairs of vertically stacked InP quantum dots *Phys. Rev. B* **76** 85338

[22] Duarte C A, da Silva E C F, Quivy A A, da Silva M J, Martini S, Leite J R, Meneses E A and Lauretto E 2003 Influence of the temperature on the carrier capture into self-assembled InAs/GaAs quantum dots *J. Appl. Phys.* **93** 627983

[23] Ma Z, Pierz K and Hinze P 2001 Abnormal temperature behavior of photoluminescence from self-assembled InAs/AlAs quantum dots *Appl. Phys. Lett.* **79** 25646

[24] Grosse S, Sandmann J H H, von Plessen G, Feldmann J, Lipsanen H, Sopanen M, Tulkki J and Ahopelto J 1997 Carrier relaxation dynamics in quantum dots: Scattering mechanisms and state-filling effects *Phys. Rev. B* **55** 44736

[25] Hiura S, Takeishi K, Urabe M, Itabashi K, Takayama J, Kiba T, Sueoka K and Murayama A 2018 Interdot spin transfer dynamics in laterally coupled excited spin ensemble of high-density InGaAs quantum dots *Appl. Phys. Lett.* **113** 023104

[26] Kalevich V K, Paillard M, Kavokin K V, Marie X, Kovsh A R, Amand T, Zhukov A E, Musikhin Y G, Ustinov V M, Vanelle E and Zakharchenya B P 2001 Spin redistribution due to Pauli blocking in quantum dots *Phys. Rev. B* **64** 45309